A High Quality Alloy718 Powder for Powder Bed Fusion Additive Manufacturing

Yusaku Maruno *
Kosuke Kuwabara **
Wang Pan ***
Sun Chen-Nan ***
Au Ka Hing Candice ***
Sin Wai Jack ***
Aw Beng Loon ***
Tan Lye King ***
Nai Mui Ling Sharon ***

* Hitachi Metals Singapore Pte. Ltd.

** Global Research & Innovative Technology Center, Hitachi Metals Ltd.

*** Singapore Institute of Manufacturing Technology, A*STAR

The limited availability of high-quality metal powder feedstocks for powder bed fusion additive manufacturing (PBFAM) is one of the factors inhibiting the adoption of this process in various industries. The present work employed PBFAM processing using a high-quality, gas atomized Alloy718 powder developed by Hitachi Metals® (HM) to fabricate high performance industrial components. A detailed comparative study of powders from HM® and from the original equipment manufacturer (OEM) was conducted. The experimental work comprised detailed powder characterizations, the development of PBFAM processes for both electron beam melting (EBM) and selective laser melting (SLM), inspection for defects and microstructural characterization of the resulting products, as well as the mechanical properties testing of printed items. The results demonstrate that the HM® powder is suitable for PBFAM and provides specimens with microstructures and mechanical properties comparable or even superior to those obtained using the OEM powder. Industrial impellers were fabricated using SLM in conjunction with the HM® powder with suitable dimensional control, and processes for the finishing of the internal and external surfaces of the impeller were devised. This work confirms that gas atomized Alloy718 powder from HM® can be employed to fabricate industrial components with complex geometries and having suitable mechanical properties.

● **Key words :** Powder-bed additive manufacturing, Selective laser melting, Electron beam melting
● **R&D Stage :** Development

1. Introduction

Additive manufacturing (AM), also known as 3D printing, is the process of creating an object in a layer-by-layer additive manner. This is the opposite of subtractive manufacturing, in which an object is created by removing material from a solid block until the final shape is obtained. AM offers design flexibility and permits parts with complex geometries to be fabricated with minimal material wastage. Increasingly, AM is being used to redesign and fabricate complex metallic industrial parts [1)~5)]. At present, the majority of research is focused on metallic materials, such as pure Cu, Ti-6Al-4V, Inconel alloys, Co-Cr alloys, steel and Ti-Al [1), 6), 7)]. However, these materials are typically provided in powdered form by the original equipment manufacturer (OEM) of the AM system and are often expensive. The limited range of material types available and high material costs thus constrain the development of AM technology. Therefore, third-party manufacturers of powders that can be provided at reasonable costs must be developed and qualified, so as to lower the total cost of AM components and enhance the competitiveness of this technology.

The present work used Alloy718, a precipitation hardened Ni-based superalloy, to conduct a detailed comparative study of powders obtained from Hitachi Metals® (HM) and an OEM. The process flow employed in this work is shown in **Fig. 1**. The current study spanned the range from powder development to the fabrication of final industrial components, employing two popular metal powder bed fusion AM technologies: selective laser melting (SLM) and electron beam melting (EBM).

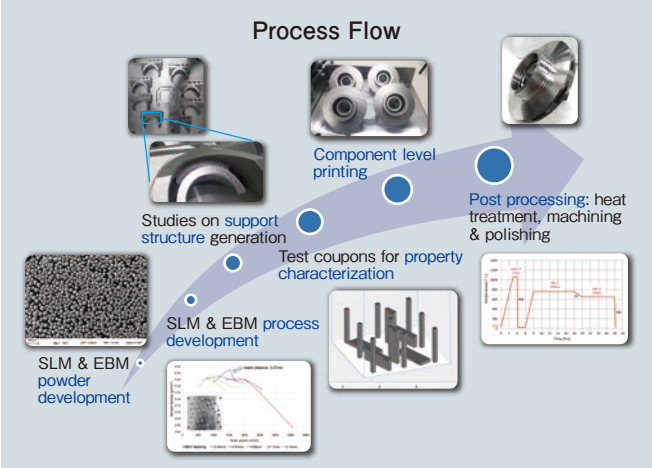

Fig. 1 The process flow in the present study

2. Experimental procedures

2.1 Powder characteristics

Pre-alloyed Ni superalloy (Alloy718) powders produced by the OEM and by HM® were used in conjunction with both SLM and EBM. Hereafter, the OEM is referred to by the equipment brand name, such that the OEM for SLM is represented by EOS* and the OEM for EBM is represented by Arcam**. These powders were characterized using different techniques [8], including laser scattering particle size distribution analysis, Hall flow meter measurements, apparent density and tapped density measurements, and scanning electron microscopy observations. The chemical compositions of these materials were determined by inductively coupled plasma atomic emission spectroscopy (ICP-AES), combustion-infrared absorbance (for C), inert gas fusion-infrared absorbance (for O), and inert gas fusion-thermal conductivity (for N).

2.2 SLM process

To examine the interactions between the various processing parameters and their effects on the sample density, it is essential to understand the concept of volumetric energy density and build rate. The volumetric energy density (E_V), which is the energy deposited per unit volume, is an important factor related to increasing the sample density. The density of energy imparted to the sample is a function of four key process parameters, as summarized by the equation

$$E_V = P/(v \cdot h \cdot t), \quad (1)$$

Where P is the laser power (W), v is the scan speed (mm/s), h is the hatch spacing (mm) and t is the powder layer thickness (mm).

Scan time is another important consideration related to adjusting the process so as to obtain a higher build rate. It has been reported that a high sample density can be achieved even when applying a faster scan rate. Units of scan time per mm^2 can be used for the build rate, which is a function of scan speed and hatch spacing, as described by the relationship

$$\text{Scan time per unit area} = \frac{\left(\frac{\text{Length}}{\text{Hatch spacing}} \times \text{Width}\right)}{\text{Scan speed}}. \quad (2)$$

In this study, only the interactions between laser power and scan speed and between hatch spacing and scan speed were investigated. An EOS* M290 system was used to conduct the SLM experiments at different laser beam powers (265, 285, 305, 315, 325, 345 and 365 W) and different hatch spacings (0.05, 0.07, 0.09, 0.11 and 0.13 mm). The associated energy densities were 20, 40, 55, 67, 85, 100 and 130 J/mm^3 as determined by back-calculating based on the scan speeds. The layer thickness was kept constant at 0.04 mm in conjunction with a platform preheating temperature of 80℃ . The samples were processed in an argon atmosphere to prevent rapid oxidation. After adjustment, the process parameters found to give the highest build rate were applied to fabricate National Institute of Standards and Technology (NIST) test pieces. The dimensions of these pieces were subsequently measured to ascertain the dimensional accuracy. These data were then used to design an industrial impeller that provided the desired degree of accuracy.

2.3 EBM process

A standard EBM process was carried out to fabricate samples, using an Arcam** A2X machine. Version 4.2 software was employed, with a 150 × 150 mm start plate, and accelerating voltage, layer thickness, speed function, line offset and focus offset values fixed at 60 kV, 75 μm, 63, 0.125 mm and 15 mA. The details of the build procedure can be found elsewhere [4]. The preheating temperature was 1,025℃ and the powder bed temperature was maintained by applying an average current of 15 mA. A 2 mm thick solid ghost box was applied to the entire

printing area and a defocused beam was employed to heat this region. This process was designed to compensate for heat loss from the start plate.

2.4 Heat treatment and materials characterization

The SLM and EBM blocks produced in this work were divided into two groups: as-built and heat-treated. (according to AMS 5664). The latter blocks were solution treated at 1,065℃ for 1 h, cooled in argon and aged at 760℃ for 10 h, cooled in a furnace to 650℃ for 2 h and finally held at 650℃ for 8 h following cooling in argon.

The densities of samples were determined using the Archimedes method. Porosity measurements were performed based on observations by optical microscopy (OM) and X-ray computed tomography (CT) [4]. Scanning electron microscopy with X-ray energy dispersive spectroscopy (SEM-EDS) and electron backscatter diffraction (EBSD) were employed for microstructural characterization. In addition, tensile tests were carried out on an Instron instrument using ASTM E8 sub-size [9] samples with a thickness of 3 mm, to evaluate the mechanical properties of the materials. In these trials, machined tensile coupons were subjected to elongation at a crosshead speed of 1 mm/min until fracture, employing a non-contact extensometer [9]. Yield strength (YS), ultimate tensile strength (UTS), elongation to fracture and Young's modulus were all calculated from the results. Surface roughness measurements were performed using a non-contact optical method.

2.5 Post-machining of the SLM-built impeller

Fig. 2 illustrates the process flow developed for the sequential post-machining of the impeller. In this process, wire cutting was used to remove external support structures from the as-printed SLM impellers. The top porous layers on these impellers had average surface roughness values, Ra, of 8 to 30 μm. CNC turning was performed to remove external porous layers and to ensure the dimensional accuracy of the final impellers. In addition, abrasive flow machining (AFM) was used to improve the internal surface finish of the as-printed SLM impellers. In this step, abrasive media accessed the rough internal and complex surfaces. These media flowed in one direction from outlet holes to inlets to prevent over-polishing of internal thin walls. **Fig. 3** presents a schematic diagram of the set of support fixtures used for mounting of the SLM impellers. These supports also guided the abrasive media flow through the intended internal holes when polishing by AFM. The fixture was fabricated from SS304 with a TiN coating for wear resistance. Additional modular fixtures were employed to ensure a uniform media flow within the internal passages during polishing. These modular fixtures also served to block the access of media through the holes that were well-polished. **Fig. 4** provides images and schematic diagrams of the modular fixtures used for internal polishing.

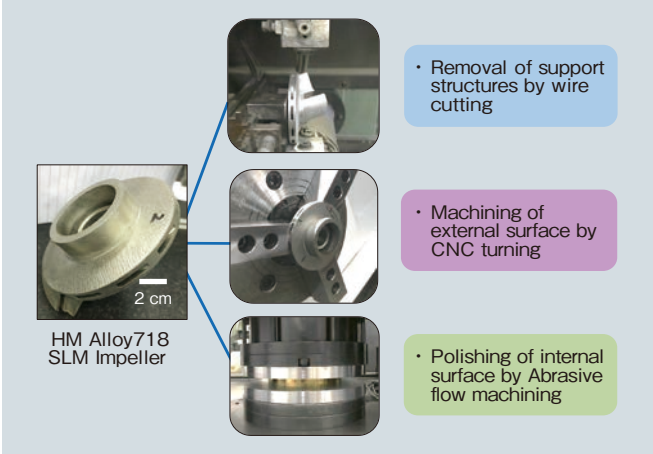

Fig. 2 The methodology employed for post-machining of SLM-built impellers

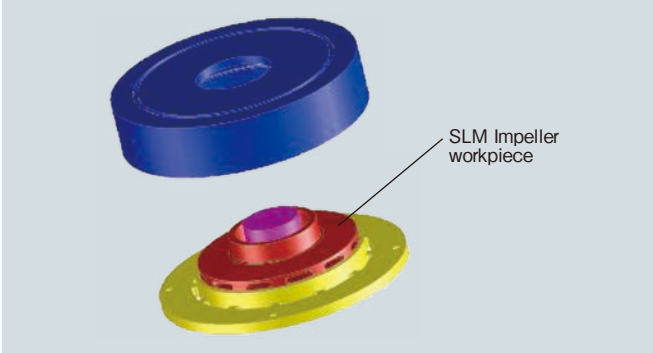

Fig. 3 A schematic diagram of the set of support fixtures used to mount the SLM-built impeller for internal polishing

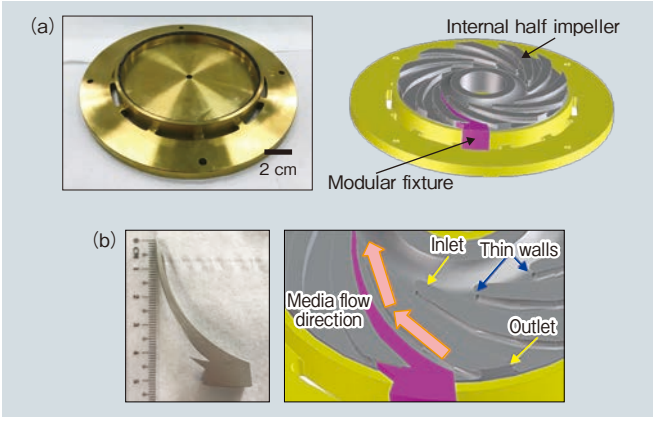

Fig. 4 Pictures and schematic diagrams of (a) base plate of AFM fixture and (b) modular fixtures used for internal polishing of SLM-built impeller

3. Results and discussion

3.1 Powder characteristics

The as-received powders exhibited a spherical morphology with a few irregular particles and a relatively high density of satellites, as demonstrated by the SEM images in Fig. 5. In addition to these satellites, spherical pores formed by gas entrapped during the atomization process were evident upon examination of cross-sections. The flowability of the HM® Alloy718 powder was excellent and comparable to that of the OEM powders, regardless of the particle size range (Table 1). In fact, the properties of this material were superior to those of the Ti-6Al-4V powder commonly used for EBM [8], suggesting that the HM® Alloy718 powder could be a suitable candidate for PBFAM. The powder packing capacity for the HM® Alloy718 was determined and an apparent density in the range of 49-60% was obtained. This value is comparable to that for the OEM powders and also similar to values for other powders currently employed in SLM or EBM processes [8), 10)]. This result suggests that the HM® Alloy718 powder is applicable to PBFAM.

Table 2 summarizes the results from chemical analysis of the as-received HM® powder as well as samples

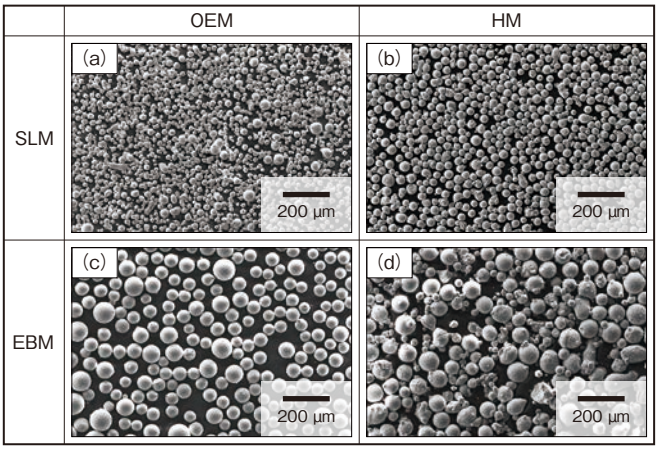

Fig. 5 Representative SEM images of various (a, c) OEM powders, (b, d) HM® Alloy718 powder, (a, b) fine powder for SLM, (c, d) coarsen powder for EBM

Table 1 PSD, hall flow rate, apparent, and tapped densities of IN718 powders with different categories. D10, D50, and D90 are the particle sizes at 10 vol.%, 50 vol.%, and 90 vol.%, respectively

Powder	D_{10} (μm)	D_{50} (μm)	D_{90} (μm)	Hall flow meter, 2.54 mm (s)	Hall flow meter, 5 mm (s)	Apparent density (g/cm^3)	Tapped density (g/cm^3)
EOS_SLM	20.23 ± 0.14	32.39 ± 0.33	53.30 ± 0.75	Does not flow	Flow after several taps	3.98 ± 0.02	4.77 ± 0.08
HM_SLM	27.53 ± 0.23	36.81 ± 0.61	51.12 ± 1.94	Does not flow	Flow after several taps	4.37 ± 0.02	5.13 ± 0.03
Arcam_EBM	54.14 ± 0.61	75.95 ± 0.85	109.24 ± 1.09	15.77 ± 0.17	NA	4.82 ± 0.03	5.24 ± 0.03
HM_EBM	59.16 ± 0.15	80.73 ± 0.19	110.91 ± 0.22	16.20 ± 0.20	—	4.43 ± 0.03	5.65 ± 0.09

Table 2 Chemical analysis results

Element	ASTM Specification (wt. %)	HM SLM Powder (wt. %)	SLM-built sample (wt. %)	HM EBM Powder (wt. %)	EBM-built sample (wt. %)
Nickel	50.0 – 55.0	52.71	52.3	52.62	52.08
Copper	0.30 (max)	<0.01	0.03	<0.01	0.03
Iron	Balance	Balance	Balance	Balance	Balance
Boron	0.006 (max)	0.0055	0.005	0.0054	0.005
Aluminum	0.20 – 0.80	0.78 *	0.80 *	0.78 *	0.80 *
Titanium	0.65 – 1.15	0.99	0.99	0.99	0.99
Tantalum + Niobium	4.75 – 5.50	5.13	5.44 *	5.18	5.09
Molybdenum	2.80 – 3.30	3.12	2.99	3.14	3.09
Cobalt	1.0 (max)	<0.01	<0.1	<0.01	<0.1
Chromium	17.0 -21.0	18.42	19.1	18.53	18.4
Sulphur	0.015 (max)	0.0003	<0.002	0.0004	<0.002
Phosphorous	0.015 (max)	N.A.	0.005	N.A.	0.005
Silicon	0.35 (max)	0.01	0.04	0.01	0.04
Manganese	0.35 (max)	<0.01	<0.01	<0.01	<0.01
Carbon	0.08 (max)	0.024	0.03	0.039	0.04
Nitrogen	N.A.	0.0016	0.003	0.0017	0.002
Oxygen	N.A.	0.0109	0.026	0.0054	0.010

fabricated from this material using SLM and EBM. The ASTM specifications for Alloy718 are also presented for comparison. The concentrations of all elements were within the specified limits, although the aluminum level was at the maximum value. These data demonstrate that the AM processing did not significantly change the chemical composition of the Alloy718.

3.2 AM Process Development

3.2.1 Selection of suitable process parameters for SLM

The sample density is plotted as a function of scan time in **Fig. 6**, which demonstrates that the density was lowered when using a rapid scan. Shorter scan times are associated with less energy being deposited, which in turn prevents proper fusion of the powder particles into fully dense components. Interestingly, the sample density was also decreased when the scan time was increased past a certain point. This occurred because the laser would dwell on a small area for an extended period of time, leading to large temperature differences and spattering, such that some material was lost.

The scan time associated with the OEM default parameters was calculated and the resulting sample density is plotted on the same chart for comparison purposes. It is evident that densities above the value achieved using the OEM default parameters could be obtained using a wide range of parameter values for the M290 system. However, the default parameters produced a suitable sample density using a shorter scan time, and only two process parameters, located in the upper left quadrant in **Fig. 6**, allow higher sample densities and faster scan times than the default parameters.

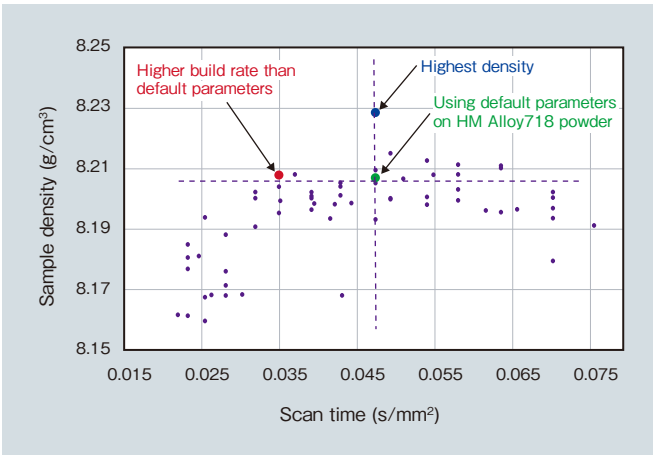

Fig. 6 Sample density versus scan time using various SLM process parameters

3.2.2 Surface roughness of AM built components

To ensure part quality, a suitable surface finish on the as-printed sample is preferable. In this work, the SLM-built samples were found to have Ra values of approximately 6.1 and 4.9 μm when using the OEM and HM® powders, respectively. In the case of the EBM-built samples, these values were 47 and 41 μm. Thus, relatively rough surfaces were obtained compared to those reported for EBM-built Ti-6Al-4V samples (approximately 25 to 35 μm) [11]. This result can be attributed to the higher build temperature of approximately 1,000℃ compared to that for the Ti-6Al-4V (650℃) and to the greater layer thickness in the present work (75 μm as compared to 50 μm). It is also worth noting that the surface roughness values for both the SLM- and EBM-built HM® samples were lower than those for the SLM- and EBM-built OEM samples. This outcome can possibly be ascribed to the narrower particle size range for the HM® Alloy718 powder. Nevertheless, it is evident that the process parameters could be further fine-tuned to improve the surface finish of the SLM-built parts.

3.2.3 Microstructures

The porosities of the samples produced by SLM demonstrated the absence of large pores and showed that the samples were close to being fully dense when using either the OEM or HM® powders. In addition, the density of the EBM-built Alloy718 using HM® powder specimen was 8.142 ± 0.044 g/cm^3, which was 99.06 ± 0.54% of the theoretical density of this material (8.22 g/cm^3). Data acquired from CT scans showed the presence of only a few pores in the EBM-built samples made using the HM® powder (**Fig. 7**). This result indicates a suitable level of fusion when employing the adjusted EBM process parameters. Some spherical pores were observed in the images, regardless of the location and geometry of the specimen, although the porosities of all samples were less than 0.12%. The appearance of some porosity is a common phenomenon in EBM-built alloys and is primarily caused by argon entrapped during the production of the gas atomized powder [12]. However, the literature and our earlier work with Ti-6Al-4V show that the presence of a limited number of small pores will not significantly affect the mechanical properties of the built part. In fact, the relative densities were calculated to be greater than

99.88%. Although more entrapped gas pores were found in the samples made with the HM® powder than in those made using the Arcam** (OEM) powder, there was no observable difference in porosity between EBM-built parts produced using either material. This lack of an effect can possibly be ascribed to the high fabrication temperature during the Alloy718 EBM process, as the long duration of the melting pool could allow bubbles to escape from the liquid.

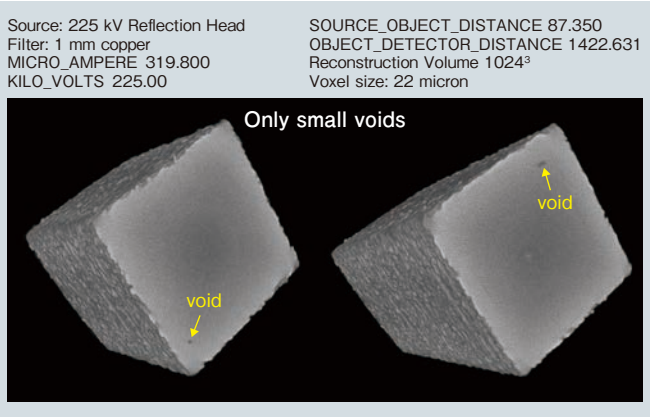

Fig. 7 CT scanning results showing minimal defects in EBM-built Alloy718 samples

As shown in **Fig. 8**, the microstructures of the SLM-built samples clearly reflect the melt pool morphology. Heat treatment also greatly altered the microstructure of the Alloy718. Within the melt pool, small dendritic structures are often generated in conjunction with a high cooling rate, and typically result in superior mechanical performance of the SLM-built parts. However, subsequent solution treatment would remove the dendritic structures and melt pool morphology. Due to the high temperature applied, grains would be expected to grow at the expense of these dendritic structures, and adversely impact hardness and mechanical strength. However, the aging heat treatment applied after the solution treatment would form strengthening precipitates (γ' and γ'') that would increase the hardness and strength of the part.

An elongated columnar structure is apparent along the side plane of the EBM-built sample, which is typical of EBM-built Alloy718 samples [13]. These columnar grains are caused by the high thermal gradient along the Z-axis [4]. It is obvious that these grains were able to grow across many layers because the build layer thickness was 75 μm. This value is different from that employed during SLM and powder-blown laser additive manufacturing [1]. Dendrites can also be found within the columnar grains. Heat treatment did not change the features of the columnar grains, in good agreement with previous reports [14]. Note also that these columnar grains appear as equiaxed grains when observed from the top plane.

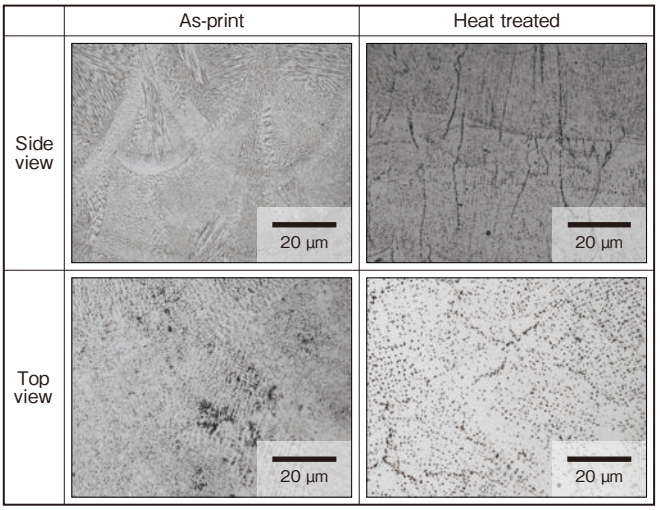

Fig. 8 Microstructures of SLM-built HM® Alloy718 specimens before and after heat treatment

3.2.4 Mechanical properties

The hardness values for SLM-built Alloy718 samples made from the HM® powder were comparable to those of specimens obtained using the EOS* powder. The EBM-built Alloy718 samples showed microhardness and macrohardness values that were higher when using the HM® material (433.7 HV and 38.1 HRC) than when using the OEM alloy (398.9 HV and 33.4 HRC). These differences may have resulted from the variations in the chemical compositions of the powders. After the 1 h solution treatment at 1,065℃ , the precipitates were dissolved into the matrix, resulting in homogeneity along the build direction. The subsequent low-temperature aging step promoted this precipitation and so further increased the hardness. Therefore, a homogeneous distribution with higher hardness values was obtained after heat treatment. Although the hardness values for the OEM samples (42 HRC) were still lower than those of the HM® samples (43.7 HRC), the difference between the two was negligible. Most importantly, the macrohardness values after heat treatment for both powder sources satisfied the standards.

The tensile test data for the SLM-built samples are shown in **Fig. 9**. These results demonstrate that the HM® Alloy718 powder yielded SLM printed parts with

mechanical properties comparable or superior to those obtained from the OEM powder. These data also show that, despite an increase in mechanical strength after heat treatment, a reduction in elongation to fracture can be observed. The effects of heat treatment and build orientation on mechanical properties in this work were found to be consistent with reports in the literature [1), 15)].

Fig. 10 provides the tensile test results obtained for EBM-built samples fabricated using the Arcam** (OEM) and HM® powders, either as-printed or heat treated. In contrast to the UTS, YS and elongation data, there are no significant variations in the Young's modulus values in the X and Y directions. It should also be noted that the Young's modulus values in the Z direction were very low (approximately 105 GPa). This value is similar to the Young's modulus of Alloy718 in the <100> direction and can likely be attributed to a significant <100> texture along the build direction. In the as-built condition, the UTS and YS values for the HM® samples were higher than those obtained from the OEM samples, although the latter specimens showed a 30% drop in elongation. Because the HM® sample had more precipitates along the grain boundaries, which increased the strength, it also exhibited premature failure along these same boundaries. After heat treatment, the UTS and YS values were increased and the elongation decreased, as expected. Interestingly, these values were comparable for both powder sources. The data were also in good agreement with results reported for Arcam** AB and satisfied the requirements of the applicable standards. This result indicates that EBM-built Alloy718 parts produced using the HM® powder had comparable tensile properties to

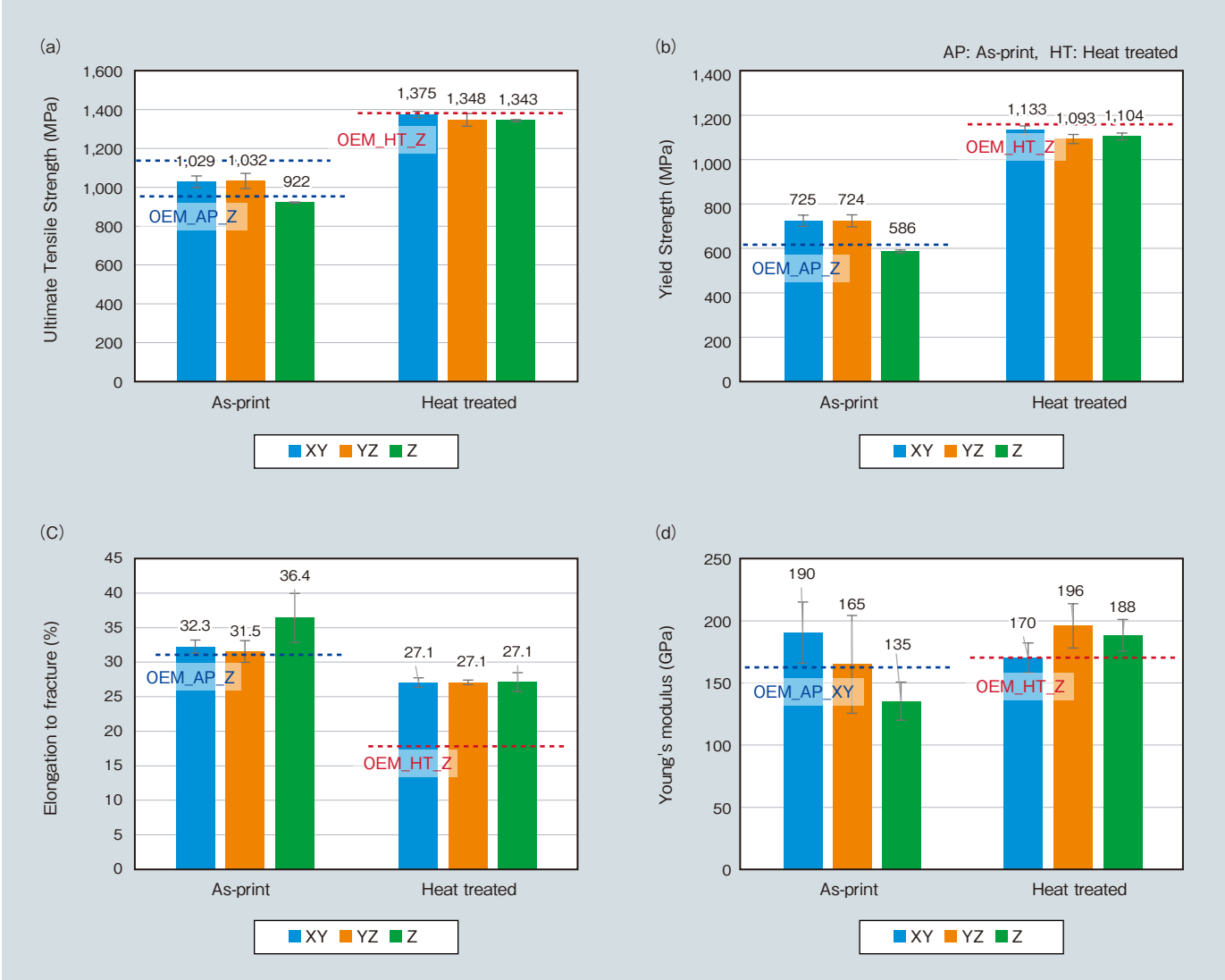

Fig. 9 Tensile properties of as-built and heat-treated SLM-built Alloy718. Bar charts showing (a) Ultimate Tensile Strength, (b) Yield Strength, (c) elongation to fracture, and (d) Young's modulus. The values from OEM [16)] were added for comparison. Note that all tensile samples were fabricated with higher build rate parameters

those of parts made using the Arcam** (OEM) powder.

The findings reported above demonstrate that the HM® Alloy718 powder was suitable as a feedstock for SLM and EBM processing to fabricate high-quality AM parts.

3.3 Dimensional testing of NIST samples and component printing by SLM using HM® powder

Dimensional accuracy measurements were performed on an NIST specimen fabricated by SLM. This sample contained several simple geometric features atop or within a diamond-shaped base. These geometries were chosen to simplify the measurements and minimize the likelihood of errors in the design file. **Fig. 11** shows the design of the test specimen and actual SLM-built sample. The measurement results indicated that the features were slightly smaller than the design values by 0.03 to 0.1 mm.

To test the developed SLM process, an industrial impeller design, which was identified as a valuable and key demo component, was provided by HM® for printing. Several batches of impellers were fabricated using SLM and post processed by heat treatment and machining to obtain the final parts. The original impeller design was

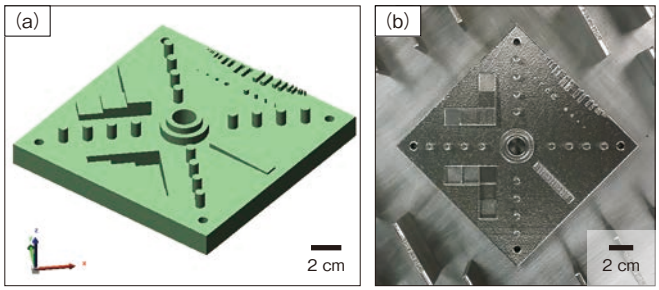

Fig. 11 SLM-built NIST artifact for dimensional accuracy testing using HM® powder. Images showing (a) 3D model, and (b) SLM-built NIST artifact

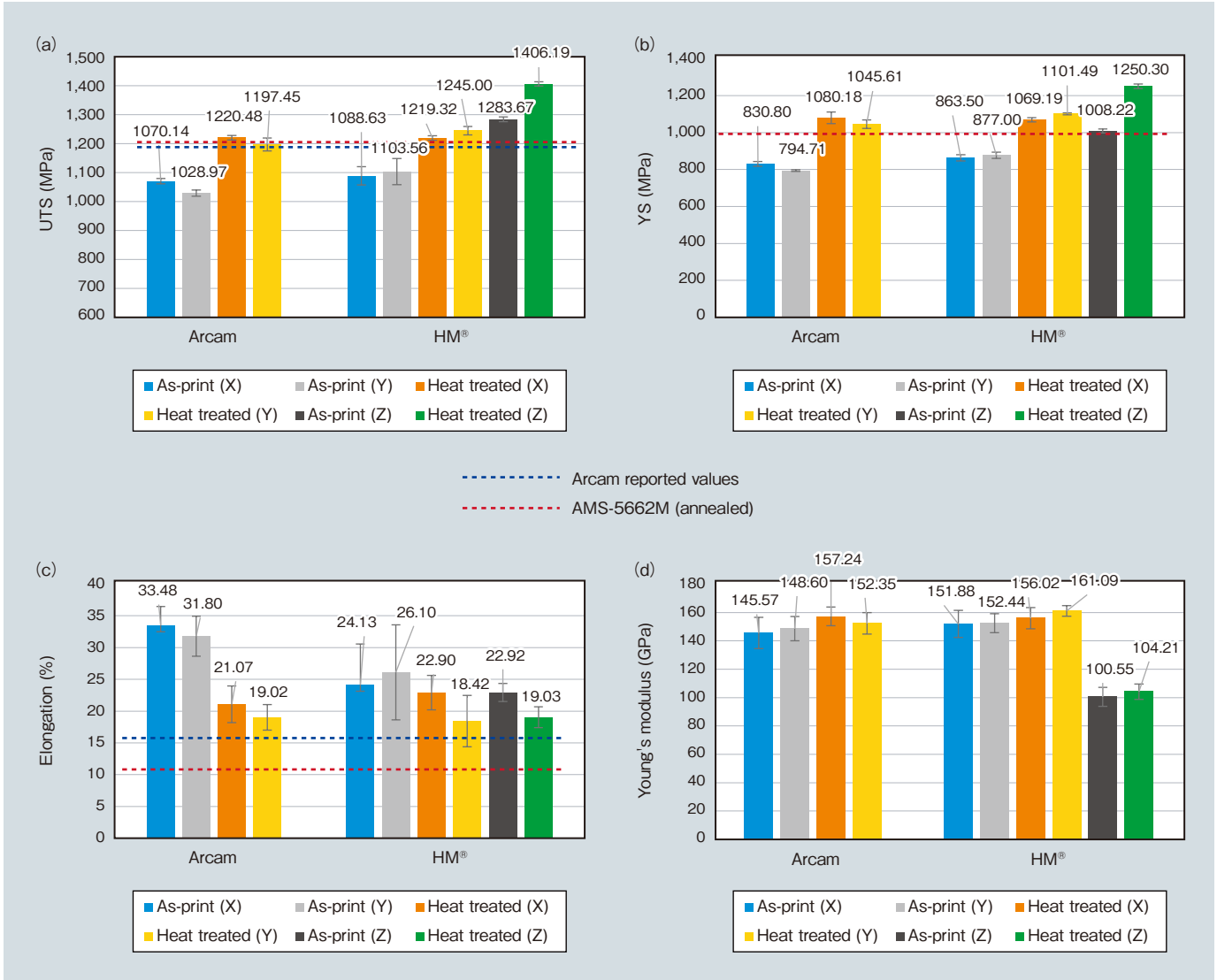

Fig. 10 Tensile properties of EBM-built Alloy718 before and after heat treatment. Bar charts showing (a) Ultimate Tensile Strength, (b) Yield Strength, (c) elongation to fracture, and (d) Young's modulus. Values for specimens made using OEM (Arcam reported values) and AMS-5662 materials are included for comparison**

modified by adding 0.5 mm to 1 mm of material to the surfaces that required machining. In addition, the length on the cylinder (**Fig. 12**) was increased from 11.5 mm to 15.5 mm in order to enable the soft jaw to clamp the sample effectively during machining.

The HM® impeller design is highly complex, with curved features, internal channels and overhanging structures. To facilitate SLM processing, suitable support structures were created and added to produce a modified impeller design that was then printed using the EOS* M290 SLM machine. **Fig. 12** provides the modified design with the support structures attached used during the file preparation stage and also presents images of a finished SLM-built HM® impeller.

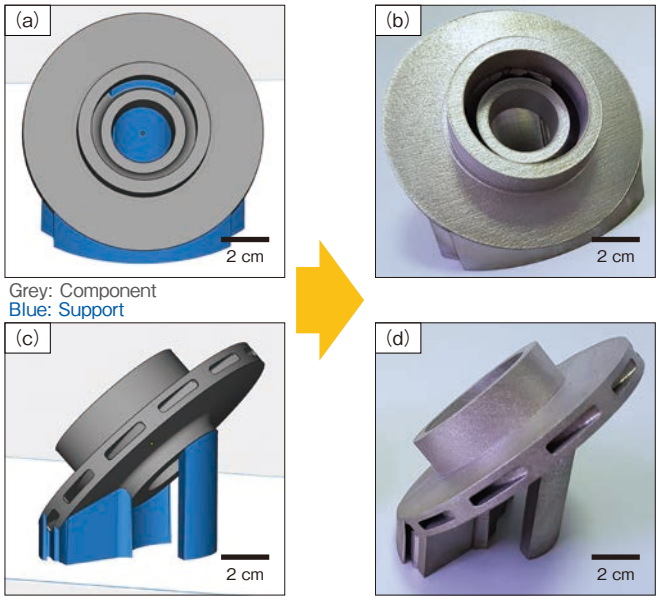

Fig. 12 Modified design with the support structures and the SLM-built impeller with HM® Alloy718. Images showing (a) model front view, (b) SLM-build part front view, (c) model side view, and (d) SLM-built part side view

3.4 Post-machining of the SLM-built component made using the HM® powder

The external surfaces of the test specimens were post-machined by CNC turning, and **Fig. 13** shows images of the as-printed SLM impeller before and after post-machining. During the CNC turning process, the external support structures remaining after wire cutting were removed along with the upper porous layers. All dimensions of each SLM impeller were machined as per the HM® design drawing.

AFM was applied to the internal surfaces to give an Ra value of 16.2 μm with a maximum of 31 μm. It should be noted that these Ra values obtained from all 12 inlet holes of the two impellers. These values were in good agreement with the results of a previous study [17]. The high as-printed roughness of these impellers is attributed to the build orientation. After polishing, the Ra of the SLM-built component was reduced significantly, to 0.67 μm.

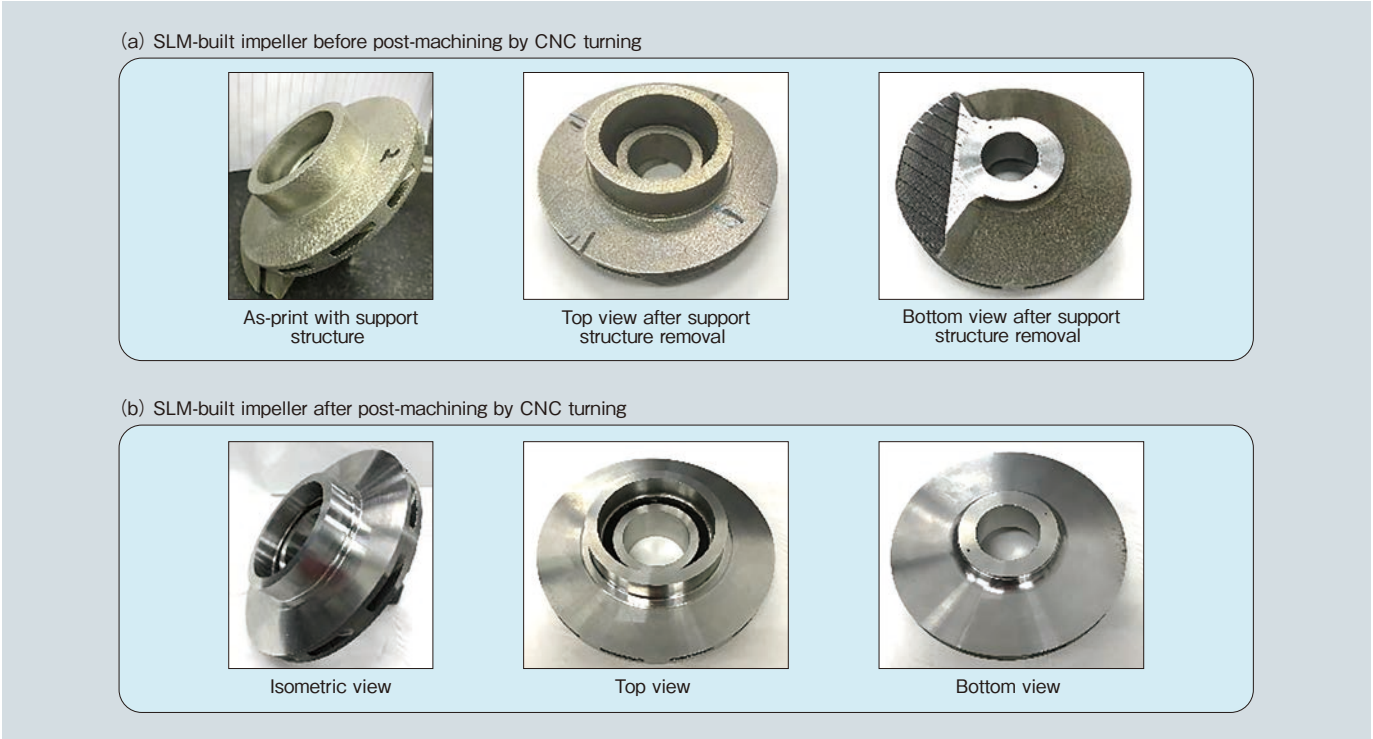

Fig. 13 SLM-built impeller (a) before and (b) after post-machining by CNC turning

4. Conclusion

PBFAM technology was employed to produce test specimens and high-value components (that is, impellers) using both OEM and HM® Alloy718 powders, as a means of evaluating these materials. The results indicate that HM® Alloy718 powder is a suitable feedstock for the fabrication of high-quality parts by either SLM or EBM. The mechanical properties obtained when using the HM® powder were comparable or even superior to those obtained from the OEM powders. An industrial impeller was fabricated by SLM using the HM® powder with good dimensional control and methods for the finishing of internal and external surfaces were developed.

References

1) T. Debroy, et al: Prog. Mater. Sci., vol. 92 (2018), p. 112.
2) P. Wang, et al: 2016 Annual International Solid Freeform Fabrication Symposium (SFF Symp 2016), Austin, Texas, USA, 2016, p. 691.
3) R. Huang, et al: J. Clean Prod., vol. 135 (2016), p. 1559.
4) P. Wang, et al: Mater. Des., vol. 95 (2016), p. 287.
5) P. Wang, M.L.S. Nai, S. Lu, J. Bai, B. Zhang, J. Wei: JOM, vol. 69 (12) (2017), p. 2738.
6) D. Herzog, et al: Acta Mater., vol. 117 (2016), p. 371.
7) D. Bourell, J.P. Kruth, M. Leu, G. Levy, D. Rosen, A.M. Beese, A. Clare: Materials for additive manufacturing, CIRP Ann. Manuf. Technol., vol. 66 (2017), P. 659.
8) P. Wang, et al: Mater. Des., vol. 168 (2019), p. 107576.
9) P. Wang, et al: J. Alloys Compd., vol. 772 (2019), p. 247.
10) Q.B. Nguyen, et al: Engineering, vol. 3 (5) (2017), p. 695.
11) P. Wang, et al: Materials, vol. 10 (10) (2017), p. 1121.
12) P. Wang, et al: Scanning optical microscopy for porosity quantification of additively manufactured components, Add. Manuf., vol. 21 (2018), p. 350.
13) D. Deng, et al: Mater. Sci. Eng., vol. A 693 (2017), p. 151.
14) Y. Kok, et al: Mater. Des., vol. 139 (2018), p. 565.
15) Y.S.J. Yoo, et al: Mater. Sci. Eng., vol. A 724 (2018), p. 444.
16) EOS: EOS NickelAlloy IN718 Data Sheet, (2014).
17) B. Zhang, et al: Mater. Des., vol. 116 (2017), p. 531.

Yusaku Maruno
ASEAN Business Planning Department,
Hitachi Metals Singapore Pte. Ltd.

Kosuke Kuwabara
Global Research & Innovative Technology Center,
Hitachi Metals Ltd.

Wang Pan
Singapore Institute of Manufacturing Technology (SIMTech),
Agency for Science, Technology and Research (A*STAR)

Sun Chen-Nan
Singapore Institute of Manufacturing Technology (SIMTech),
Agency for Science, Technology and Research (A*STAR)

Au Ka Hing Candice
Singapore Institute of Manufacturing Technology (SIMTech),
Agency for Science, Technology and Research (A*STAR)

Sin Wai Jack
Singapore Institute of Manufacturing Technology (SIMTech),
Agency for Science, Technology and Research (A*STAR)

Aw Beng Loon
Singapore Institute of Manufacturing Technology (SIMTech),
Agency for Science, Technology and Research (A*STAR)

Tan Lye King
Singapore Institute of Manufacturing Technology (SIMTech),
Agency for Science, Technology and Research (A*STAR)

Nai Mui Ling Sharon
Singapore Institute of Manufacturing Technology (SIMTech),
Agency for Science, Technology and Research (A*STAR)